Comprehensive proteomic and metabolomic analysis uncover the response of okra to drought stress

Jiyue Wang [Corresp., 1], **Denghong Shi** [1], **Yu Bai** [1], **Ting Zhang** [1], **Yan Wu** [1], **Zhenghong Liu** [1], **Lian Jiang** [1], **Lin Ye** [1], **Zele Peng** [1], **Hui Yuan** [1], **Yan Liu** [Corresp. 1]

[1] Guiyang University, Guiyang, China

Corresponding Authors: Jiyue Wang, Yan Liu
Email address: acute2803764@126.com, Liuyan19680607@126.com

The response of okra to drought stress is very complicated, the molecular mechanisms underlying this process remains ambiguous up to now. In this study, different degrees of water-stress responses of okra leaf were explained by using transcriptomics and metabolomic approaches. The photosynthesis and glycometabolism in okra leaf were both adversely affected by drought stress, leading to inhibition of carbohydrate metabolic process, and then influencing the secondary plant metabolism. Further, drought stress disturbed amino acid metabolism, especially for tyrosine-derived pathway as well as arginine and proline metabolism, which have been shown to be significantly enriched under water withholding conditions based on multi-omics conjoint analysis (transcriptome, proteome and metabolome). In-depth analysis of the internal linkages between differentially expressed transcripts, proteins, and metabolites decidedly indicate that tyrosine metabolism could confer tolerance to drought stress by influencing carbon and nitrogen metabolism. These findings provide a whole framework of the regulation and relationships of major transcripts and peptides related to secondary metabolism, particularly , the role of critical proteins and metabolite involved in the change of amino acid metabolism in response to drought stress.

Comprehensive proteomic and metabolomic analyses uncover the response of okra to drought stress

Jiyue Wang[1*], Denghong Shi[1], Yu Bai[1], Ting Zhang[1], Yan Wu[1], Zhenghong Liu[1], Lian Jiang[1], Lin Ye[1], Zele Peng[1], Hui Yuan[1], Yan Liu[1#]

1. Guiyang University, Guiyang, China.
*Corresponding author: acute2803764@126.com,
#Co-corresponding author: Liuyan19680607@126.com

Abstract:

The response of okra plants to drought stress is very complicated, and the molecular mechanisms involved are currently unknown. In this study, the response of okra plants to different degrees of water stress were explained using proteomic and metabolomic approaches. The photosynthesis and glycometabolism of okra leaves were both adversely affected by drought stress, leading to the disruption of the carbohydrate metabolic process, impacting secondary plant metabolism. Drought stress also disturbed amino acid metabolism, especially in the tyrosine-derived pathway as well as arginine and proline metabolism, which have both been shown to be significantly enriched under water withholding conditions based on multi-omics conjoint analyses (transcriptome, proteome, and metabolome). An in-depth analysis of the internal connections between differentially expressed transcripts, proteins, and metabolites indicate that tyrosine metabolism could confer drought stress tolerance to okra plants by influencing carbon and nitrogen metabolism. These findings provide an understanding of the regulation and relationships of the major transcripts and peptides related to secondary metabolism, especially the role of the critical proteins and metabolites involved in the amino acid metabolism changes that occur in response to drought stress.

Key word: Okra (*Abelmoschus esculentus* L. Moench); Water stress; Protein expression profile; Metabolome

1. Introduction

Okra (*Abelmoschus esculentus* L. Moench), which belongs to the Malvaceae family, originated in Africa and India and is able to adapt to a wide range of warm climates (Gemede et al., 2016). Okra is an important, healthy vegetable and is very popular in various parts of the world. The value of one ton of okra varies worldwide, with 2017 prices ranging from $236.8 USD in Mexico to $3,870.6 USD in Fiji. A series of studies have shown that okra polysaccharide could be used as a potential immunomodulator for the treatment of diabetic nephropathy (Chen et al., 2016; Peng et al., 2016). The rhamnogalacturonan polysaccharide found in okra is also associated with hypoglycemic effects (Liu et al., 2018).

The growth and development of plants is often compromised by abiotic stresses such as drought. Plants undergo substantial changes in their physiological and biochemical systems when faced with water deficiency (Farias et al., 2019). Recent studies have shown that under drought conditions, the biomass of okra as well as the uptake of phosphorus in its shoot were both significantly reduced, while nitrogen, potassium, iron, and zinc levels increased in the shoot (Müller et al., 2019). Water deficits affect the physiology and development of okra, and severe water shortages can significantly reduce okra production. Improving okra irrigation techniques and cultivating a new drought-resistant variety of okra are two effective ways to solve this problem. Amin et al (Amin et al., 2009) found that a 1mM concentration of salicylic acid and ascorbic acid can considerably mitigate the physical damage to plants caused by drought stress.

In recent years, the rise of omics studies has provided an important means of revealing the response of plants to biotic or abiotic stress. The molecular mechanisms underlying OsDRAP1-mediated salt tolerance in rice was revealed through comparative transcriptome and metabolome analyses (Wang et al., 2021). Li et al (Li et al., 2021) reported the mechanisms at play in the molecular and physiological metabolic response of N. sibirica to salt stress by using comprehensive transcriptome and metabolome profiling. Bavaresco et al (Bavaresco et al., 2020) found that protein hydrolysates modulate the leaf proteome and metabolome of grapevines in response to water stress. The mechanism of Se accumulation and tolerance in C. violifolia was also identified using metabolome, transcriptome, and proteome technologies (Rao et al., 2021). The protein turnover and regulatory classes of proteins and metabolites in Medicago truncatula during drought stress and subsequent recovery were identified through an integration of proteome and metabolome analyses (Lyon et al., 2016).

Previous studies on okra have focused mainly on the characterization of its genotypes (Ghevariya & Mahatma, 2017), its medical applications (Erfani et al., 2018), its agronomic characteristics (Meldrum et al.,

2018), and its edible quality (Petropoulos et al., 2018). However, few studies report on the molecular mechanism of resistance to drought stress in okra plants. The aim of this study is to reveal the drought-resistant mechanism of okra at the molecular level. The protein expression and metabolic profiles of okra under different water withholding conditions were obtained using a multi-omics analysis. The functional proteins and metabolites associated with drought tolerance, and the metabolic pathways involved were also identified using a proteomic analysis and a metabolomics analysis, respectively.

Materials and Methods

Plant Materials

A drought-tolerant okra cultivar called 'Xianzhi' was selected based on a previous physiological and biochemical experiment (Wang et al., 2018). It was then cultivated in a greenhouse at the Guiyang University in Guizhou province, China. Blades from seedling cuttings were used to extract total proteins and metabolites.

Drought stress treatment

Drought treatment was carried out in a constant temperature incubator. Okra plants were planted in plastic buckets 20.0 cm in height with a 15.0 cm inner diameter. They were cultivated for 35 days at 70% humidity and a temperature of 25± 2 °C. First, the okra plants were planted by direct seeding into a basin containing nutrient-enriched soil. After sprouting, the seedlings were watered every 2 days. Then, after an adaptation period of two weeks, a dehydration treatment was applied to all plants. Leaves were collected from the seedlings after 0 days, 5 days, 7 days, 15 days, and 20 days of water withholding. The collected leaves were then kept in liquid nitrogen for protein extraction and stored at -80 ℃ in an ultra-low temperature refrigerator. The five different drought treatments were marked as P1, P2, P3, P4, and P5, respectively, with samples taken from each drought treatment. Using a randomized block design, 11 pots were used in each treatment with three used for proteomic assays and the other eight for metabolomic analysis.

Sample processing and TMT quantification

The protein was extracted using the methods described by Xiong et al., 2019. After trypsin digestion (where a protease inhibitor was added at a rate of 50:1), 8M urea was added and an ultrasound was performed for 1s, and then stopped for 2s, with that pattern repeated for a total of 20s. After centrifugation at 14,000g for 20 min, 5 μL of the supernatant was kept for quantification, and the rest was frozen at -80 ℃. The protein concentration was determined using the Bradford method. SDS-page was performed using 20 μg of each sample with Coomassie blue staining for 30 min followed by decolorization until the background was clear. FASP (Filter

Aided Sample Preparation) was then carried out using a TMT® kit (Thermo Scientific, USA). After enzymatic digestion, 41 μL of TMT reagent was added to a 100μg sample (100μL per sample), and incubated at room temperature for 1 h. Then, 8 μL of 5% quenching reagent (Thermo Scientific, USA) was added and incubated for 15 min to stop the reaction. The mixed and labeled samples were centrifuged to the bottom of the tube by vortex, and then dried with centrifugal vacuum freezing.

Peptide pre-separation and LC-MS/MS analysis

The tryptic peptides were dissolved in solvent A (2% acetonitrile, PH 10) to 100 μL, then centrifuged at 14,000g for 20 min, and the supernatant was removed and put into a custom-made reverse-phase analytical column (Durashell-C18, 4.6 mm×250 mm, 5 μm, 100 A). It took five minutes for solvent B to move from 5% to 8% (98 % acetonitrile, PH 10), an additional 30 minutes for it to grow from 8% to 18%, another 27 minutes for it to reach 32%, and then just two minutes for it to move from 32% to 95%. The 95% held for 4 minutes and then decreased all the way to 5% in the next 4 minutes, all at a constant flow rate of 0.7 ml/min on an RIGOL L-3000 high performance liquid chromatography system (Beijing Puyuan Jing Electric Technology Co., LTD).

The components obtained from high pH reversed phase separation were redissolved in reagent with 2% methanol and 0.1% formic acid, centrifuged at 12,000 g for 10 minutes, and then the supernatant was loaded onto an EASY-Spray column (12 cm x 75 μm, C18, 3 μm). The loading pump was running for 15 min at a flow rate of 350 nL/min. Peptides were separated using the EASY-nLC 1000 System (Nano HPLC, Thermo) at a constant flow rate of 600 nL/min. The separation gradient is shown in Table 1.

The peptides were then injected into an NSI ion source for ionization and analyzed using Orbitrap Fusion Lumos (Thermo) mass spectrometry. The ion source voltage was set to 2.0 kV, and the capillary temperature was 320 °C. The mass spectrometer scan range was set to 300-1400 m/z, and the scan resolution was set to 120,000 FWHM. The full scan automatic gain control (AGC) target, and full scan Max.IT (maximum implantation time) were set to 5.0 e^5 and 50 ms, respectively. The dd-MS2 resolution was set to 60,000 FWHM and 35% fragmentation energy was used for fragmentation according to the higher energy collision dissociation (HCD) method. The automatic gain control (AGC) target was set to 5.0e^4, and the Max.IT was set to 118 ms.

The resulting MS/MS data were then analyzed using the Proteome Discoverer (v.2.1). The tandem mass spectra were searched against the *Abelmoschus esculentus* L. corresponding transcriptome database (Shi et al., 2020) and the UniProt/NCBI database. The enzyme digestion method was set as trypsin; the max missed cleavages was set as 2; the tolerances of precursor ion mass and fragment ion mass were set as 15 ppm and 20

ppm, respectively; the static modification and dynamic modification were set as C carboxyamidomethylation (57.021 Da) and M Oxidation (15.995 Da), respectively; and the quantitative method was set as iTRAQ-6plex.

Peptide identification and differentially expressed protein (DEP) screening

The peptides produced through the enzymatic hydrolysis of the proteins were identified through mass spectrometry, and then the putative protein was obtained using a bioinformatics analysis. In order to evaluate the overall picture of the proteomic data, the physical and chemical properties were detected at both the peptide and protein levels. For peptides, this meant calculating: peptide length, PSM number distribution, score distribution for identified peptides, and missed cleavage distribution for identified peptides. For proteins: distribution of identified peptide numbers for proteins, distribution of PSM numbers matched to proteins, MW distribution for identified proteins, coverage distribution for identified proteins, and pI distribution of identified proteins were all calculated.

Since the sample was repeated ≥ 2 times, a t-test was used for differential analysis. DEPs were defined with a P-value of < 0.05, and a fold change (FC) of > 1.2 between any two treatments.

Functional annotation of proteins

The Clusters of Orthologous Groups (COG) analysis was achieved by Blasting KYVA sequences. The Gene Ontology (GO) and The Kyoto Encyclopedia of Genes and Genomes (KEGG) annotations were acquired using *Arabidopsis Thaliana* annotated data in Uniprot. The PPI (Protein-Protein Interaction Networks) analysis used *Arabidopsis Thaliana* data in the STRING database to search the relationship between the DEPs and their possible functional groups.

An enrichment analysis was used to determine the over-expressed genes or proteins, allowing further analyses to identify the functional categories or pathways involved. An over-representation analysis was used to perform a statistical significance test according to hypergeometric distribution. The P values and false discovery rate (FDR) values (based on multiple hypothesis testing) of the enrichment degree from differential proteins were calculated based on the functional categories of GO and Go Slim as well as the KEGG Pathways; the smaller the P value or FDR value, the higher the enrichment degree.

The GO analysis was scattered, and it was difficult to draw overall conclusions based on the overly complex and detailed classification results. However, GO Slim is a simplified version of GO, which matches most entries to a few parent entries, making it easy to obtain the protein number and enrichment degree contained in each large entry. Like the GO analysis, the GO Slim annotation is divided into three major categories: biological process (BP), cellular component (CC), and molecular function (MF).

Protein-protein interaction (PPI) analysis

The identified DEPs were used to construct the PPI network to explore the inter-class relationships and possible functional groups of the DEPs. STRING (Search Tool for the Retrieval of Interacting Genes/Proteins) is part of the Elixir infrastructure, and is one of Elixir's core data resources. The DEPs were uploaded to the STRING 11.0 database (https://string-db.org/), and the interacting proteins were identified based on *Arabidopsis*

thaliana as the model organism. Protein-protein interactions were identified using a combined score of 0.4 as the threshold. The Cytoscape 3.6.1 software (Shannon et al., 2003) was used to visually construct the protein interaction network.

Metabolite extraction

The metabolites were extracted according to the De Vos RC1 method (De Vos et al., 2007) and the approach of Sangster et al., 2006. Each of the treatments, containing 6 replicates, were used for this metabolomic analysis. After weighing, 200 mg (±2%) of each sample was put in a 2 mL EP tube, 0.6 mL 2-chlorophenylalanine (4 ppm) methanol (-20 ℃) was added, and then the sample was vortexed for 30 seconds. After that, 100 mg glass beads were added to each sample and the samples were put into the TissueLysis II tissue grinding machine and ground at 25 Hz for 60 s, followed by an ultrasound at room temperature for 15 minutes. The samples were then centrifuged at 25 ℃ for 10 min at 1,750g, and the supernatant was filtered through a 0.22 μm membrane to obtain the samples necessary for LC-MS. A 20 μL quality control sample was taken from each sample (Fig. S1) and used to monitor deviations in the analytical results from the pool mixtures and compare them to the errors caused by the analytical instrument itself. The remaining part of each sample was used for LC-MS detection.

LC-MS analysis

Chromatographic separation was completed with a ThermoUltimate 3000 system equipped with an ACQUITY UPLC® HSS T3 (150×2.1 mm, 1.8 μm, Water) column maintained at 40 ℃. The temperature of the autosampler was set to 8 ℃. Gradient elution of analytes was implemented with 0.1% formic acid in water (C) and 0.1% formic acid in acetonitrile (D) or 5 mM ammonium formation water (A) and acetonitrile (B) at a flow rate of 0.25 mL/min with 2μL of each sample injected after equilibration. An increasing linear gradient of solvent B (v/v) was carried out as specified in the manufacturer's instructions.

The ESI-MSn experiments were performed on the Thermo Q Exactive mass spectrometer with a spray voltage of 3.8 kV and -2.5 kV in positive and negative modes, respectively. Auxiliary gas and sheath gas were set at 10 and 30 arbitrary units, respectively. The capillary temperature was set at 325 ℃. The analyzer scanned over a mass range of m/z 81-1,000 for full scan at a mass resolution of 70,000. The data dependent acquisition of the MS/MS spectra was carried out using an HCD scan. The normalized collision energy was set to 30 eV. Dynamic exclusion was used to remove unnecessary information from the MS/MS spectra. The original data obtained by the ProteWizard software (V3.08789) was converted into the mzXML format. The XCMS program of R was used to carry out peak identification, peak filtration, and peak alignment, leading to the building of the data

matrix including mass to change ratio (m/z), retention time (r/t), and intensity. The original LC-MS data of the metabolites were standardised and used for the principal component analysis (PCA), partial least squares discriminant analysis (PLA-DA), and orthogonal projections to latent structures-discriminant analysis (OPLA-DA). The metabolomics profiles were investigated as described by Zhong *et al* (Zhong et al., 2022). Differential metabolites (DMs) were identified according to *P*-value (P >0.05) from a two-tailed Student's t-test on the normalised peak areas. The pheatmap program package in R (V3.3.2) was used to carry out agglomerative hierarchical clustering. A pathway enrichment analysis was carried out using the KEGG database with P-values <0.05 considered a significant enriched pathway. A correlation analysis of the differential metabolites was also performed in this study.

Results

Protein identification and evaluation

A total of 18,875 peptides aligning to 4,151 proteins were identified by means of TMT analysis. The results were highly reliable in detecting the physiological-biochemical properties of the identified peptide and its presumptive protein (Fig. S2-10), which could then be used for subsequent analysis.

DEP identification and functional description

Quantitative values of different labels in the PD search results were directly extracted, and the global view of the DEPs (Fig. 1) was obtained after removing the results with 0 value. DEPs were identified through pairwise comparison between the different treatments (after 0 days, 5 days, 7 days, 15 days, and 20 days of water withholding). Ten sample pairs and the number of DEPs identified in the pairwise comparison of each sample pair are shown in Figure 2: P2 versus P1 (126 DEPs), P3 versus P1 (363 DEPs), P4 versus P2 (1,015 DEPs), P4 versus P1 (791 DEPs), P4 versus P2 (46 DEPs), P4 versus P3 (245 DEPs), P5 versus P1 (261 DEPs), P5 versus P2 (170 DEPs), P5 versus P3 (159 DEPs), and P5 versus P4 (236 DEPs). Most of the DEPs identified were shared among the ten pairs. In particular, the number of DEPs found between each treatment and the control (P1) first increased and then decreased with increased levels of water stress. The number of DEPs between 15 days of dehydration (P4) and the control (P1) was the most abundant, followed by P5 versus P1, and then P3 versus P1. However, the number of DEPs found among the different drought treatments were less the number found between each treatment and control. For example, a total of 363 DEPs were found in P3 versus P1, but only 46 DEGs were found in P3 versus P2. Moreover, the number of down-regulated DEPs found between each treatment and control was higher than between the different treatments. More up-regulated DEPs were found in P4 versus P2, P5 versus P2, P4 versus P3, P5 versus P3, and P4 versus P5 than were found in P3 versus P2.

All the differentially expressed proteins that were identified were annotated by aligning them to the COG database, which identifies lineal homologous genes through an extensive comparison of protein sequences from a wide variety of organisms. A total of 2,818 DEPs were grouped into 25 COG categories (Fig. 3). The largest category was “general function prediction only” containing 406 DEGs (14.41%), followed by “posttranslational modification, protein turnover, chaperones” (393 DEGs, 13.95%), “translation, ribosomal structure and biogenesis” (259 DEGs, 9.19%), “energy production and conversion” (221 DEGs, 7.8%), and “carbohydrate transport and metabolism” (205 DEGs, 7.27 %). Only four DEPs were assigned to the “cell motility” category and eight to the “cytoskeleton” category. In addition, there were 70 DEPs assigned to “function unknown,” accounting for 2.24%.

GO analysis of DEPs

According to the results of the enrichment analysis, all DEPs in the ten pairs (P2 versus P1, P3 versus P1, P3 versus P2, P4 versus P1, P4 versus P2, P4 versus P3, P5 versus P1, P5 versus P2, P5 versus P3, and P5 versus P4) were classified into 1,809 subgroups of biological process (BP), 438 subgroups of cellular component (CC), and 1,341 subgroups of molecular function (MF). Fig. 4 shows the top 20 GO categories of all DEPs. The “response to cadmium ion” was the largest BP category, involving 286 DEPs. There were 1,225 DEPs involved in “chloroplast,” which was the largest CC category, and the “structural constituent of ribosome” was largest MF category, including 243 DEPs. Furthermore, all DEPs were involved in 17 cellular component categories, 7 molecular function categories, and 24 biological process categories through a GO Slim analysis. In this analysis, the largest BP category was “transport” (420 DEPs), the largest CC category was “cytoplasm” (3,025 DEPs), and the largest MF category was “metal ion binding” (875 DEPs; Fig. 5). The GO Slim analysis of DEPs was also performed in the ten pairs (P2 versus P1, P3 versus P1, P3 versus P2, P4 versus P1, P4 versus P2, P4 versus P3, P5 versus P1, P5 versus P2, P5 versus P3, and P5 versus P4) with “metal ion binding” as the largest MF category for all ten sample pairs. There were 27, 73, 11, 238, 57, 37, 181, 71, 39, and 46 DEPs enriched in “metal ion binding” in P2 versus P1, P3 versus P1, P3 versus P2, P4 versus P1, P4 versus P2, P4 versus P3, P5 versus P1, P5 versus P2, P5 versus P3, and P5 versus P4, respectively. The largest CC category was also “cytoplasm,” with 100, 259, 39, 752, 178, 128, 597, 199, 120, and 177 DEPs enriched in each of the ten pairs, respectively. The largest BP category differed by pair: “carbohydrate metabolic process” was the largest in P3 versus P1 (30), P4 versus P1 (93), P5 versus P1 (75), P3 versus P2 (6), P4 versus P2 (54), P5 versus P2 (26), P4 versus P3 (15), and P5 versus P4 (22); “signal transduction” was the largest in P2 versus P1 (19); and “transport/Reproduction”

was the largest in P5 versus P3 (13). More down-regulated GO terms were found in P2 versus P1, P3 versus P1, P3 versus P2, and P5 versus P1, with the other pairs having more up-regulated GO terms than down-regulated.

KEGG pathway of DEPs

The KEGG enrichment analysis of the DEPs showed that 125 metabolic pathways were obtained from all DEPs, 37 of which were significantly ($P < 0.01$) enriched KEGG pathways (Table 2). There were seven pathways with enrichment values > 10: "metabolic pathways," "carbon metabolism," "carbon fixation in photosynthetic organisms," "biosynthesis of amino acids," "biosynthesis of secondary metabolites," "photosynthesis," and "pyruvate metabolism" (Table S1). In addition, 50 KEGG pathways were enriched in P2 versus P1, 81 in P3 versus P1, 27 in P3 versus P2, 110 in P4 versus P1, 79 in P4 versus P2, 71 in P4 versus P3, 102 in P5 versus P1, 79 in P5 versus P2, 57 in P5 versus P3, and 65 in P5 versus P4, as shown in Fig. S21-S30. Among the ten sample pairs, the top three enriched pathways were "metabolic pathways," "biosynthesis of secondary metabolites," and "biosynthesis of amino acids." There were more down-regulated DEP pathways than up-regulated in P2 versus P1, P3 versus P1, P3 versus P2, and P4 versus P1, and more up-regulated DEP pathways in the rest of the sample pairs (Table S2). Interestingly, up-regulated DEP pathways linked to "protein processing in endoplasmic reticulum" were found in P4 versus P3, and in P5 versus P3 (Fig. S31-32), while "ribosom" was the predominant pathway of up-regulated DEPs in P2 versus P1, P3 versus P1, P4 versus P1, and P5 versus P1. The main pathways of the down-regulated DEPs in all ten sample pairs were "metabolic pathways" and "biosynthesis of secondary metabolites."

PPI network for exploring hub proteins associated with drought stress responses in okra

In order to search potential proteins associated with drought stress responses, all DEPs in four pairs (P2 versus P1, P3 versus P1, P4 versus P1, P5 versus P1) were used to construct the PPI network. Four large networks with several smaller networks were obtained from the DEPs in these four sample pairs with 86 DEPs involved in protein interaction in P2 versus P1, 284 DEPs in P3 versus P1, 884 DEPs in P4 versus P1, and 679 DEPs in P5 versus P1. Among these interacting proteins, more down-regulated DEPs were detected in all of these pairs except in P4 versus P1.

The four large networks obtained from the P2 versus P1, P3 versus P1, P4 versus P1, and P5 versus P1 pairs are shown in Figure 6. The large P2 versus P1 network contained 114 nodes linking 335 edges (Fig. 6A); the P3 versus P1 network comprised 313 nodes connecting 2,202 edges (Fig. 6B); the P4 versus P1 network had 828 nodes and 17,798 edges (Fig. 6C); and the P5 versus P1 network had 660 nodes linking 9,767 edges (Fig. 6D). The key nodes were obtained through selecting nodes with a high betweenness centrality (BC) value (BC value>

0.02) or a large degree (D) value (D value >10). In P2 versus P1, 30 nodes had a high BC value, 29 nodes had a large degree value, and 14 nodes had both a large BC and degree value; in P3 versus P1, 15 nodes had a high BC value, 118 had a large degree value, and 15 nodes had both a large BC and degree value; in P5 versus P1, 15 nodes had a high BC value, 592 nodes had a large degree value, and seven nodes had both a large BC and degree value; and in P5 versus P1, 439 nodes had a high BC value, 11 nodes had a large degree value, and 10 nodes had both a large BC and degree value (Table 3). Among the nodes with both a large degree and high BC value, TPI was shared in all four pairs, AT3G29320 was shared between three pairs (P2 versus P1, P3 versus P1, P4 versus P1), CDC5 was shared between three pairs (P3 versus P1, P4 versus P1, P5 versus P1), TP1 was shared between three pairs (P2 versus P1, P3 versus P1, P4 versus P1), NRPB2 and GAPC1 were shared between two pairs (P2 versus P1, P3 versus P1), GS2 was shared between two pairs (P3 versus P1, P5 versus P1), and P5CS2 was shared between two pairs (P2 versus P1, P4 versus P1). TPI is a protein with both the highest BC value and CC value, and emb1473 is a protein with the largest degree in the network of P2 versus P1. TPI had a degree value of 19, and occupied the central position in the network because of its high degree, BC, and CC values. TPI was also considered to be centrally located in the network of P4 versus P1, and P5 versus P1 due to its high degree, BC, and CC values in those networks. In the network of P3 versus P1, the RPL4 protein encoded by AT5G02870 had the largest degree value, the CDC5 protein had the highest BC value, and the Hsp70b protein had the highest CC value. In the P3 versus P1 network, the CDC5 protein had a degree value of 40 and a CC value of 0.41441441, and occupied the central position. In the P4 versus P1 network, the PRPL3 protein encoded by AT2G43030 had degree value of 184, the largest in the network. The CDC5 protein had the highest BC value in P4 versus P1, and in P5 versus P1. These results indicate that these proteins play a vital role in these large networks.

Identification of differential metabolites

Based on the results of the QC and QA analyses (Fig. S33), all samples exhibited a high quality, and could be used for subsequent screening and identification of differential metabolites (DMs). According to the PCA, the components of the five samples (P1, P2, P3, P4, P5) displayed effective separation (Fig. 7A, B). As a supervised method, a PLS-DA (Partial Least Squares Discriminant Analysis), the most commonly used classification method in metabonomics, was performed to confirm the PCA results. PLS-DA also has potential applications in sample classification. Satisfactory modeling and prediction results were obtained from all sample comparison groups despite low Q2 values, suggesting metabolomes are distinguishable under water-deficit conditions (Fig. 8A, B, C, D). In addition, the OPLS-DA (orthogonal partial least squares-discriminant analysis) showed a remarkable separation among the five samples (Fig. 7C, D). Furthermore, based on the parameter VIP (variable

of importance in prediction) >1, which is a measure of the variable importance in the OPLS-DA, a total of 1,422 differential metabolites (DMs) were identified in all five samples, which were displayed as a heat map (Fig. 7E). The detailed information of the DMs from this 6-sample group comparisons (P2 versus P1, P3 versus P1, P4 versus P1, P5 versus P1, P3 versus P2, and P4 versus P2) are shown in supplementary table S3-8. The number of DMs in the P4 versus P1 group was the highest, whereas the P3 versus P2 group had the lowest number of DMs, which is similar to the DEP results (Fig .9). More up-regulated DMs were identified through metabolomic analysis compared to the DEPs identified from the same samples through RNA-seq based transcript profiling. The metabolite levels of five comparison groups are shown in supplementary Figure S34. A total of five metabolites,including Ubiquinone-1, perrlly aclohol, phosphoserine, d-Limonene, and 2-Amino-2-dexy-D - gluconate, exhibited higher levels in samples under water withholding conditions compared to control.

KEGG pathways of DMs

A total of 331 DMs from all five samples were identified in the KEGG database: 95 DMs were found in P2 versus P1, 60 DMs in P3 versus P1, 172 DMs in P4 versus P1, 135 DMs in P5 versus P1, 53 DMs in P3 versus P2, and 82 DMs in P4 versus P2 (Supplementary table S 9-14). There were 22, 11, 41, 32, 1, and 9 up-regulated DMs with a fold change >5 in each pair, respectively. Among them, ubiquinone-1 and xanthoxic acid were shared in P2 versus P1, P3 versus P1, P4 versus P1, and P5 versus P1, and L-isoleucine was shared in P3 versus P2 and P4 versus P2. Some DMs were only found in the samples under water-deficient conditions. Dimethyl sulfone was unique to the samples after 5 days (P2), 15 days (P4), and 20 days (P5) of water withholding. Xanthine, dihydrouracil, and 13(S)-HOT were only observed in the P2 and P4 samples. The accumulation of some DMs was reduced in samples under conditions of water deficiency compared to controls, including: 3-methylthiopropionic acid, cyclic AMP, 3-dehydroshikimate, L-arginine, CMP, 3-hydroxyphenylacetic acid, galactose 1-phosphate, and deoxycytidine. Based on the pathway enrichment assessment, tyrosine metabolism was the only significantly enriched pathway (FDR<0.05, pathway impact values ≥ 0.2) in the P5 versus P1 group comparison (Supplementary table S12). The only significantly enriched pathway in the P3 versus P2 group comparison was arginine and proline metabolism (Supplementary table S13), whereas the rest of group comparisons had no significantly enriched pathways. Tyrosine metabolism includes nine components: 6 up-regulated MDs (3,4-dihydroxyphenylethyleneglycol, 3,4-dihydroxy-L-henylalanine, L-tyrosine, succinate semialdehyde, dopamine, fumarate, acetoacetate, 4-hydroxy-phenylacetaldehyde) and one down-regulated MD (tyramine; Supplementary Table S12). A total of 11 components were linked to arginine and proline metabolism: glyoxylate, L-Ornithine, L-glutamate, L-proline, L-1-pyrroline-3-hydroxy-5- carboxylate, S-adenosyl-L-

methionine, L-arginine, pyruvate, hydroxyproline, (4R)-4-hydroxy-2-oxoglutarate, and spermidine (Supplementary Table S13). Furthermore, a correlation analysis of the differential metabolites showed that ubiquinone-1 accumulation was the most positively correlated to L-tyrosine accumulation, and xanthoxic acid content was positively correlated with ubiquinone-1 and L-tyrosine in the P5 versus P1 group. L-tyrosine composition in the P5 versus P1 group was also negatively correlated with cyclic AMP, 3-dehydroshikimate, CMP, 3-hydroxypheny-lacetic acid, and deoxycytidine. In the P3 versus P2 group, a significant positive correlation was found between L-proline and L-isoleucine accumulation. As a marked osmotic modulation in response to drought stress, the proline accumulation in each sample was investigated more closely. L-Proline showed a significant accumulation after 20 days of water withholding (P5) compared with control (P1; Supplementary Table S6) and 4-Hydroxyproline content was increased in P3 versus P1, and in P4 versus P1 (Supplementary Table S4, S5). The concentration of 4-hydroxyproline and L-proline were both increased in P3 versus P2, and in P4 versus P2 (Supplementary Table S7, S8).

Discussion

The decline of photosynthesis and glycometabolism-related proteins and metabolites resulting in water stress.

Water stress affects protein biosynthesis and degradation, and the photosynthetic process (Amin et al., 2009). Similar to those found in wheat (Michaletti et al., 2018), some photosynthetic-related proteins, mainly photosystem II oxygen-evolving enhancer protein 1, photosystem I reaction center subunit (psaK), photosystem II Psb27 protein, and ribulose-bisphosphate carboxylase, were down-regulated in samples under water deficiency conditions. The expression patterns of these proteins were confirmed in our study by the significant reduction of sorbitol observed during water stress, which is the main end-product of photosynthesis, and is essential for stamen development in apple trees (Meng et al., 2018). However, the levels of photosystem I subunit IV and photosystem II oxygen-evolving enhancer protein 2 increased in water deficit conditions, implying these substrates, components of the photosynthetic system, exhibit different roles in response to photosynthesis impairment induced by drought stress. As reported in the water-stressed leaves of apple trees (Yang et al., 2019), a significant reduction in photosynthesis is generally correlated with changes in sugar metabolism.

In this study, six of the top KEGG pathways connected to glycometabolism were also influenced by water stress, including glycolysis/gluconeogenesis, pyruvate metabolism, glyoxylate and dicarboxylate metabolism, citrate cycle (TCA cycle), fructose and mannose metabolism, and the pentose phosphate pathway. Declines were mainly seen in ribose 5-phosphate isomerase A, alpha-N-acetylglucosaminidase, pyruvate dehydrogenase E1 component alpha subunit [EC:1.2.4.1], triosephosphate isomerase (TPI), and glycosyltransferase (AT3G29320).

TPI occupied the central position in both the P4 versus P1 network and the P5 versus P1 network due to its high degree, BB, and CC values, as it plays an important role in the glycolysis pathway. A recent study in *Barley* indicated TPI could be linked to drought tolerance in a comparative proteome-transcriptome analysis (Wójcik-Jaga et al., 2020). However, the expression pattern of the TPI protein was not consistent with the direction of changes seen in transcript accumulation during water stress. This could be partly due to the instability of transcripts, which are prone to RNAse degradation (Wójcik-Jaga et al., 2020). For the glycosyltransferase gene, the pattern of changes in protein and transcript accumulation was very similar under water stress conditions. Zheng *et al.,* (Zheng et al., 2017) confirmed that QUA1, which has been identified as a glycosyltransferase in *Arabidopsis*, increases drought tolerance by regulating chloroplast-associated calcium signaling. Similar findings have also been shown in rice (*Oryza sativa* L.; Dinesh et al., 2017). The following pathways involved in carbohydrate metabolism were found to be down-regulated in our KEGG-based metabonomics analyses despite high FDR values: fructose and mannose metabolism, glyoxylate and dicarboxylate metabolism, pyruvate metabolism, glycolysis/gluconeogenesis, pentose phosphate pathway, and starch and sucrose metabolism. These results are not only consistent with our proteome data, but also match the results of previous transcriptome analyses (Shi et al., 2020). Similar results have also been observed in other plants, such as *Medicago truncatula* (Lyon et al., 2016) and spring-wheat (Michaletti et al., 2018).

The disturbance of amino acid metabolism was induced by water stress.

Most DEPs identified in this study were enriched in "biosynthesis of secondary metabolites" and "biosynthesis of amino acids," which is consistent with previous RNA-seq results (Shi et al., 2020). However, only "tyrosine metabolism" and "arginine and proline metabolism" were considered significantly enriched pathways in our metabolomic analysis. It is well known that secondary metabolism is critical to plant growth and development, and can be induced by both biotic and abiotic stresses (Fox et al., 2017). The involvement of secondary metabolites in response to drought stress is extremely complicated and depends on various parameters, such as high temperature and photoinhibition, which typically accompany drought stress (Niinemets & Way, 2016). Previous studies have demonstrated that water deficiency can damage the biosynthesis of secondary metabolites in plants, interfering with normal growth and generating chlorosis, which reduces plant production or even causes the plant to die (Afshar et al., 2012; Bitarafan et al., 2019). Transcriptomic analyses have shown that secondary metabolism in plants is regulated by a large number of transcription factors, most of which belong to the bHLH, MYB, MYB-like, C2H2, and bZIP families and are down-regulated during water stress (Shi et al., 2020). The down-regulation of MYB-related transcription factor LHY (MYB-like families) and transcription

406 factor MYC2 (bHLH families) in drought conditions have been further confirmed using proteomic approaches,
407 suggesting that they might be pivotal candidate genes for subsequent verification.

408 This study also found that the reduction in proteins linked to secondary metabolites mainly involved NADH-
409 dependent glutamate synthase 1 isoform 1 (K00264 glutamate synthase (NADPH/NADH) [EC:1.4.1.13
410 1.4.1.14]), lipoxygenase (K00454 lipoxygenase [EC:1.13.11.12]), allene oxide synthase, (K01723
411 hydroperoxide dehydratase [EC:4.2.1.92]), and the peroxidase superfamily protein (K00430 peroxidase
412 [EC:1.11.1.7]). The genes corresponding to these proteins all had reduced expression levels except the
413 peroxidase superfamily protein.Four genes related to glutamate synthase (NADPH/NADH) [EC:1.4.1.13
414 1.4.1.14]) were down-regulated in the water shortage samples (P5); this down-regulation aligned with the
415 reduction of L-glutamic content during water stress. The NADH-dependent glutamate synthase (NADH-
416 GOGAT), which uses NADH as the electron donor, is present mostly in non-photosynthesizing cells, where the
417 reductant is supplied by the pentose phosphate pathway (Forde & Lea, 2007). The importance of NADH-
418 GOGAT in ammonium assimilation has previously been reported in various species (Konishi et al., 2014), as
419 well as its potential links to drought response through amino acid metabolism. It has been demonstrated that
420 disruptions in the amino acid metabolism of plants can be attributed to decreases in NADH-GOGAT activity
421 (Forde & Lea, 2007). A special regulation mode of amino acid metabolism associated with drought stress
422 tolerance has been reported in wheat (Aidoo et al., 2017), *Lotus japonicus* (Sanchez et al., 2012), and maize
423 plants (Alvarez et al., 2008). A total of 20 types of amino acids were obtained in our metabonomics analysis
424 (Supplementary Table S15). The changes in the patterns of the different amino acids varied under different water
425 stress conditions, similar to the changes observed in the *Lotus japonicus* species (Sanchez et al., 2012) and in
426 maize plants (Alvarez et al., 2008). Phosphoserine content increased in all water shortage samples compared
427 with control, and the concentration of both L-arginine and L-glutamic acid decreased. Notably, the L-proline
428 content, which is a well-known bio-marker for water deficit, was significantly higher in the sample after 20 days
429 of water withholding (P5) compared with control (P1), but this increase was not observed in the other water
430 shortage samples. An accumulation of 4-hydroxyproline was observed in P3 versus P1, and in P4 versus P1,
431 while the arginine and proline metabolism pathway, which involves 11 components, was only enriched in P3
432 versus P2. Among these 11 components, L-proline and 4-hydroxyproline amounts were increased in samples
433 after seven days of water withholding (P3). Proline changes are associated with extreme water scarcity in many
434 plant species (Witt et al., 2012; Pirzad et al., 2011), but these changes are genotype specific and also related to
435 the extent of the water stress (Bowne et al., 2012). Proline is known as a compatible solute essential for osmotic

adjustments. It protects cellular structures during water stress and also plays an important role in ROS (reactive oxygen species) scavenging (Shorangiz et al., 2014), thus alleviating the adverse effects of drought stress on plant metabolism. It is thus reasonable to conclude that disturbances in the amino acid metabolism observed in this study was due to the enhanced protein breakdown induced by corresponding down-regulated genes.

The tyrosine-derived pathway is important for drought tolerance.

Our results highlight the importance of tyrosine metabolism, which was a unique significantly enriched pathway in the comparison of water stress conditions (P5) and control (P1) in our study. As a key enzyme in the tyrosine-derived pathway, tyrosine aminotransferase (TAT) catalyzes the reversible interconversion of tyrosine and 4-hydroxyphenylpyruvate for the biosynthesis of secondary metabolites. According to a previous transcriptome analysis (Shi et al., 2020), the TAT gene is up-regulated during water deficit, which is in agreement with the corresponding enzyme in our proteomic analysis. A recent study in apple trees (*Malus domestica*) found the same accumulation pattern of ubiquinone-1 in the metabolome, reinforcing the hypothesis that TAT genes confer drought tolerance (Hwa et al., 2018). Ubiquinone (UQ) is an important prenyl quinone whose core cyclic scaffold is provided by the tyrosine-derived pathway. UQ functions as an electron transporter in the respiratory chain and is indispensable in a plant's response to abiotic stress (Liu & Lu, 2016). We found a significant accumulation of dopamine after 20 days of water withholding compared to control. Some studies have reported that dopamine confers drought tolerance in plants. According to a correlation analysis of metabolites, the contents of dopamine and ubiquinone-1 were all significantly positively correlated with L-tyrosine accumulation, implying that okra plants could improve resistance to drought and prevent drought-induced damage by enhancing tyrosine metabolism and its derivatives.

We observed significant decreases in the abundance of glutamine synthetase (GS) proteins after 7 days and 20 days of water withholding. The corresponding GS gene was also down-regulated in water stress samples. The decline of L-glutamic acid during water stress was consistent with the expression pattern of the GS gene and protein. GS2 was also shown to be important in protein interaction networks because of its large degree and high BC values. The reduction of L-glutamic acid observed could be linked to tyrosine metabolism accumulation and the synthesis of arginine. Similar findings have been reported in the metabolome of wheat (Michaletti et al., 2018). Glutamic acid (Glu) can supply amino groups for photorespiratory metabolism, and also ornithine to produce arginine (Arg) for carbon (C) and nitrogen (N) assimilation and partitioning (Díaz et al., 2005). GS is also known as a metabolic indicator for drought stress tolerance in wheat (Nagy et al., 2013), which is further supported by previous studies of GS protein abundance in many plant species (Wang et al., 2018). Water stress

conditions affects the balance between photosynthetic carbon uptake and the use of photoassimilates, causing alterations in the sugar pools (Michaletti et al., 2018). This further supports the hypothesis that tyrosine metabolism could confer drought tolerance to plants by influencing carbon and nitrogen metabolism. Further research should focus on the regulation mechanism of the GS2-mediated protein interaction network in the response of okra plants to drought stress.

Conclusion

Comparing transcriptomic, proteomic, and metabolomic data showed an obvious connection between all three, especially the metabolome and proteome. Water stress disrupts the biosynthesis of secondary metabolites, especially in amino acid metabolism, which is associated with the inhibition of photosynthesis and glycometabolism. The components of the tyrosine-derived pathway play key roles in improving drought tolerance in okra plants.

Author Contributions: Sample collection and processing: Lian Jiang, Lin Ye, Zele Peng, Hui Yuan. Experiment: Jiyue Wang, Yu Bai, Denghong Shi. Data analysis: Jiyue Wang, Yu Bai, Yan Wu, Ting Zhang, Zhenghong Liu. Project design and writing: Jiyue Wang, Yan Liu. All authors also share responsibility for the content of the article.

Figure 1 Heat map of all DEPs among five samples
Figure 2 Statistics of DEPs from the ten sample pairs: P2 versus P1, P3 versus P1, P3 versus P2, P4 versus P1, P4 versus P2, P4 versus P3, P5 versus P1, P5 versus P2, P5 versus P3, and P5 versus P4. Red: up-regulated expressed proteins, blue: down-regulated expressed proteins.
Figure 3 COG functional classification of all DEPs. Different colors represent different categories in the COG database.
Figure 4 Top 20 GO categories of all DEPs
Figure 5 The most enriched GO terms in GO Slim
Figure 6 Illustration of the PPI network
A: The network of P2 versus P1, B: The network of P3 versus P1, C: The network of P4 versus P1, D: The network of P5 versus P1. Network nodes represent proteins. Edges represent protein-protein associations. The green nodes represent down-regulated DEPs, red nodes represent up-regulated DEPs. The size of the node indicates its degree value: the larger the radius, the greater the degree value.
Figure 7 A: PCA score plot in positive ion mode. B: PCA score plot in negative ion mode. C: OPLS-DA score plot in positive ion mode. D: OPLS-DA score plot in negative ion mode. E: 10 Statistics of DMs from six sample pairs: P2 versus P1, P3 versus P1, P3 versus P2, P4 versus P1, P4 versus P2, and P5 versus P1. Red: up-regulated expressed proteins, blue: down-regulated expressed proteins.
Figure 8 PLS-DA score plot and permutation test plot
A: PLS-DA score plot in positive ion mode. B: PLS-DA score plot in negative ion mode.
C: OPLS-DA permutation test plot in positive ion mode. D: OPLS-DA permutation test plot in negative ion mode.
Figure 9 The heat map of differential metabolites among five samples. The columns represent samples, the rows represent metabolites, and different colors indicate the relative content of the differential metabolites.

Supplementary data

Figure S1 Metabolite extraction
Figure S2 Peptide length statistics
Figure S3 PSM number distribution
Figure S4 Score distribution for identified peptides
Figure S5 The distribution of missed cleavage sites for the identified peptides
Figure S6 Peptide-to-protein distribution
Figure S7 The distribution of PSM numbers for each protein
Figure S8 MW distribution of the identified proteins
Figure S9 The coverage distribution for the identified proteins
Figure S10 The pI distribution of the identified proteins
Figure S11-20 Enriched GO terms of the ten sample pairs based on proteomic analysis
Figure S21-30 KEGG Pathways of the ten sample pairs based on proteomic analysis
Figure S31 KEGG Pathway enrichment of up-regulated DEPs in P4 versus P3
Figure S32 KEGG Pathway enrichment of up-regulated DEPs in P5 versus P3
Figure S33 QC (A) and QA (B) analysis of all samples
Figure S34 The metabolite levels in five comparison groups (P2 versus P1, P3 versus P1, P3 versus P2, P4 versus P1, P4 versus P2, P5 versus P1). Different colors represent different samples.
Figure S34 The principal component analysis from six sample pairs (P2 versus P1, P3 versus P1, P3 versus P2, P4 versus P1, P4 versus P2, P5 versus P1.)
Table S1 The pathways with enrichment values >10
Table S3-8 The DMs identified in the six sample pairs
Table S9-14 KEGG Pathway enrichment of six sample pairs based on the metabonomics analysis
Table S15 Expression of identified amino acids in four comparison groups (P2 versus P1, P3 versus P1, P4 versus P1, P5 versus P1)

References:

Afshar et al.(2012) Afshar, K., Gürbüz, B., and Uyanik, M. Biotic and abiotic stresses mediated changes in secondary metabolites induction of medicinal plants. *Tibbi Ve Aromatik Bitkiler Sempozyumu*. 2012.

Aidoo et al.(2017) Aidoo, M.K., Quansah, L., Galkin, E., Batushansky, A., Wallach, R., Moshelion, M., Bonfil, D.J., and Fait, A. A combination of stomata deregulation and a distinctive modulation of amino acid metabolism are associated with enhanced tolerance of wheat varieties to transient drought. *Metabolomics*. 2017; 13: 138. doi:10.1007/s11306-017-1267-y

Alvarez et al.(2008) Alvarez, S., Marsh, E.L., Schroeder, S.G., and Schachtman, D.P. Metabolomic and proteomic changes in the xylem sap of maize under drought. *Plant, Cell & Environment* . 2008;31:325-340. doi:10.1111/j.1365-3040.2007.01770.x

Amin et al.(2009) Amin, B., Mahleghah, G., Mahmood, H., and Hossein, M. Evaluation of Interaction Effect of Drought Stress with Ascorbate and Salicylic Acid on Some of Physiological and Biochemical Parameters in Okra (Hibiscus esculentus L.). *Research Journal of Biological Sciences.* 2009. doi:http://dx.doi.org/

Bavaresco et al.(2020) Bavaresco, L., Lucini, L., Squeri, C., Zamboni, M., and Frioni, T. Protein hydrolysates modulate leaf proteome and metabolome in water-stressed grapevines. *Scientia Horticulturae.* 2020;109413. doi:10.1016/j.scienta.2020.109413

Bitarafan et al.(2019) Bitarafan, Z., Asghari, H.R., Hasanloo, T., Gholami, A., Moradi, F., Khakimov, B., Liu, F., and Andreasen, C. The effect of charcoal on medicinal compounds of seeds of fenugreek (Trigonella foenum-graecum L.) exposed to drought stress. Industrial Crops and Products. 2019;131:323-329. doi:10.1016/j.indcrop.2019.02.003

Bowne et al.(2012) Bowne, J.B., Erwin, T.A., Juttner, J., Schnurbusch, T., Langridge, P., Bacic, A., and Roessner, U. Drought responses of leaf tissues from wheat cultivars of differing drought tolerance at the metabolite level. *Molecular Plant*. 2012;5:418-429. doi:10.1093/mp/ssr114

Chen et al.(2016) Chen, H., Jiao, H., Cheng, Y., Xu, K., Jia, X., Shi, Q., Guo, S., Wang, M., Du L, and Wang, F. In Vitro and In Vivo Immunomodulatory Activity of Okra (Abelmoschus esculentus L.) Polysaccharides. *Journal of Medicinal Food*. 2016;19:253-265. doi:10.1089/jmf.2015.3513

De Vos et al.(2007) De Vos, R.C., Moco, S., Lommen, A., Keurentjes, J.J., Bino, R.J., and Hall, R.D. Untargeted large-scale plant metabolomics using liquid chromatography coupled to mass spectrometry. *Nature Protocols* . 2007;2:778-791. doi:10.1038/nprot.2007.95

Díaz et al.(2005) Díaz, P., Borsani, O., Márquez, A., and Monza, J. Nitrogen metabolism in relation to drought stress responses in cultivated and model Lotus species. *Lotus Newsletter*. 2005;35(1):83-92

Dinesh et al.(2017) Dinesh, A., Hariprasanna, K., Vanisri, S., Sujatha, M., and Dangi, K. In silico Identification of Genes for Combined Drought and Salinity Stress in Rice (Oryza sativa L.). *Advances in Research* . 2017;9:1-8. doi:10.9734/AIR/2017/32041

Erfani et al.(2018) Erfani, M.N., Tabandeh, M.R., Shahriari, A., and Soleimani, Z. Okra (Abelmoscus esculentus) Improved Islets Structure, and Down-Regulated PPARs Gene Expression in Pancreas of High-Fat Diet and Streptozotocin-Induced Diabetic Rats. *Cell Journal.* 2018;20:31-40. doi:10.22074/cellj.2018.4819

Farias et al.(2019) Farias, D., Silva, P., Lucas, A., Freitas, M., and Junior, L. Physiological and productive parameters of the okra under irrigation levels. *Scientia Horticulturae*. 2019; 252. doi:10.1016/j.scienta.2019.02.066

Forde et al.(2007) Forde, B.G., and Lea, P.J. Glutamate in plants: Metabolism, regulation, and signalling. *Journal of Experimental Botany*. 2007;58:2339-2358.doi.org/10.1093/jxb/erm121

Fox et al.(2017) Fox, H., Doron-Faigenboim, A., Kelly, G., Bourstein, R., and David-Schwartz, R. Transcriptome analysis of Pinus halepensis under drought stress and during recovery.*Tree Physiology*. 2017; 38, 423-441. doi:10.1093/treephys/tpx137

Gemede et al.(2016) Gemede, H.F., Haki, G.D., Beyene, F., Woldegiorgis, A.Z., and Rakshit, S.K. Proximate, mineral, and antinutrient compositions of indigenous Okra (Abelmoschus esculentus) pod accessions: implications for mineral bioavailability. *Food Science & Nutrition.* 2016;4:223-233. doi:10.1002/fsn3.282

Ghevariya et al.(2017) Ghevariya, T.V., and Mahatma, L. Molecular characterization of Okra yellow vein mosaic virus infecting okra in south Gujarat. *Plant Disease Research*. 2017;32,206-210

Hwa et al.(2018) Hwa, B., Qd, A., Dd, A., Shuang, Z.A., Ml, A., Svna, C., Fm, A., and Ke, M.A. Comprehensive genomic analysis of the tyrosine aminotransferase (tat) genes in apple (malus domestica) allows the identification of mdtat2 conferring tolerance to drought and osmotic stresses in plants. *Plant Physiology and Biochemistry*. 2018; 133, 81-91. doi:10.1016/j.plaphy.2018.10.033

Konishi et al.(2014) Konishi, N., Ishiyama, K., Matsuoka, K., Maru, I., Hayakawa, T., Yamaya, T., and Kojima, S. NADH−dependent glutamate synthase plays a crucial role in assimilating ammonium in the Arabidopsis root. *Physiologia Plantarum*. 2014;152(1):138-151. doi:10.1111/ppl.12177

Li et al.(2021) Li, H., Tang, X., Yang, X., and Zhang, H. Comprehensive transcriptome and metabolome profiling reveal metabolic mechanisms of Nitraria sibirica Pall to salt stress. *Scientific Reports*. 2021; 11(1):12878. doi:10.1038/s41598-021-92317-6

Liu et al.(2016) Liu, M.M., and Lu, S.F. Plastoquinone and Ubiquinone in Plants: Biosynthesis, Physiological Function and Metabolic Engineering. *Frontiers in Plant Science* 2016. doi: 10.3389/fpls.2016.01898

Liu et al.(2018) Liu, J., Zhao, Y., Wu, Q., John, A., Jiang, Y., Yang, J., Liu, H., and Yang, B. Structure characterisation of polysaccharides in vegetable "okra" and evaluation of hypoglycemic activity. *Food Chemistry*. 2018; 242:211-216. doi:10.1016/j.foodchem.2017.09.051

Lyon et al.(2016) Lyon, D., Castillejo, M.A., Mehmeti-Tershani, V., Staudinger, C., Kleemaier, C., and Wienkoop, S. Drought and Recovery: Independently Regulated Processes Highlighting the Importance of Protein Turnover Dynamics and Translational Regulation in Medicago truncatula. *Molecular & Cellular Proteomics*. 2016;15:1921-1937. doi:10.1074/mcp.M115.049205

Meldrum et al.(2018) Meldrum, G., Padulosi, S., Lochetti, G., Robitaille, R., and Diulgheroff, S. Issues and Prospects for the Sustainable Use and Conservation of Cultivated Vegetable Diversity for More Nutrition-Sensitive Agriculture. *Agriculture* .2018;8(7), 112. doi.org/10.3390/agriculture8070112

Meng et al.(2018) Meng, D., He, M., Bai, Y., Xu, H., Dandekar, A.M., Fei, Z., and Cheng, L. Decreased sorbitol synthesis leads to abnormal stamen development and reduced pollen tube growth via an MYB transcription factor, MdMYB39L, in apple (Malus domestica). *New Phytologist* . 2018;217:641-656. doi: 10.1111/nph.14824

Michaletti et al.(2018) Michaletti, A., Naghavi, M.R., Toorchi, M., Zolla, L., and Rinalducci, S. Metabolomics and proteomics reveal drought-stress responses of leaf tissues from spring-wheat. *Scientific Reports*. 2018, 8(1):5710. doi:10.1038/s41598-018-24012-y

Müller et al.(2019) Müller, A., Eltigani, A., and George, E. The abundance of arbuscular mycorrhizal fungal species in symbiosis with okra plants is affected by induced drought conditions in a calcareous substrate. *Rhizosphere.* 2019;10. doi:10.1016/j.rhisph.2019.100150

Nagy et al.(2013) Nagy Z, Németh E, Guóth A, Bona L, Wodala B, Pécsváradi A. Metabolic indicators of drought stress tolerance in wheat: Glutamine synthetase isoenzymes and Rubisco. *PLANT Plant Physiology and Biochemistry* . 2013;67:48-54. doi:10.1016/j.plaphy.2013.03.001

Niinemets et al.(2016) Niinemets, Ü., and Way, D. Uncovering the hidden facets of drought stress: secondary metabolites make the difference. *Tree Physiology*. 2016;129-132. doi:10.1093/treephys/tpv128

Peng et al.(2016) Peng, C.H., Chyau, C.C., Wang, C.J., Lin, H.T., Huang, C.N., and Ker, Y.B. Abelmoschus esculentus fractions potently inhibited the pathogenic targets associated with diabetic renal epithelial to mesenchymal transition. *Food & Function*. 2016, 7(2):10.1039. doi:10.1039/c5fo01214g

Petropoulos et al.(2018)Petropoulos, S., Fernandes, A., Barros, L., and Ferreira, I. Chemical composition, nutritional value and antioxidant properties of Mediterranean okra genotypes in relation to harvest stage. *Food Chemistry*. 2018; 242, 466-474. doi:10.1016/j.foodchem.2017.09.082

Pirzad et al.(2011) Pirzad, A., Shakiba, M.R., Zehtab-Salmasi, S., Mohammadi, S.A., and Samadi, A. Effect of water stress on leaf relative water content , chlorophyll , proline and soluble carbohydrates in Matricaria Chamomilla L. *Journal of Medicinal Plants Research* . 2011;5(12), 2483-2488. doi:10.1016/j.jep.2011.04.064

Rao et al.(2021) Rao, S., Yu, T., Cong, X., Lai, X., Xiang, J., Cao, J., Liao, X., Gou, Y., Chao, W., Xue, H., Cheng, S., and Xu, F. Transcriptome, proteome, and metabolome reveal the mechanism of tolerance to selenate toxicity in Cardamine violifolia. *Journal of Hazardous Materials*. 2021;406:124283. doi:10.1016/j.jhazmat.2020.124283

Sanchez et al.(2012) Sanchez, D.H., Schwabe, F., Erban, A., Udvardi, M.K., and Kopka, J. Comparative metabolomics of drought acclimation in model and forage legumes. *Plant, Cell & Environment.* 2012;35(1):136-149. doi:10.1111/j.1365-3040.2011.02423.x

Sangster et al(2006) Sangster, T., Major, H., Plumb, R., Wilson, A.J., and Wilson, I.D. A pragmatic and readily implemented quality control strategy for HPLC-MS and GC-MS-based metabonomic analysis. *Analyst*. 2006;131(10):1075-1078. doi:10.1039/b604498k

Shannon et al(2003) Shannon, P., Markiel, A., Ozier, O., Baliga, N.S., Wang, J.T., Ramage, D., Amin, N., Schwikowski, B., and Ideker, T. Cytoscape: a software environment for integrated models of biomolecular interaction networks. *Genome Research*. 2003;13(11):2498-2504. doi:10.1101/gr.1239303

Shi et al(2020) Shi, D.H., Wang, J.Y., Bai, Y., and Liu, Y. 2020. Transcriptome sequencing of okra (Abelmoschus esculentus L. Moench) uncovers differently expressed genes responding to drought stress. *Springer India*. 2020(2). doi:10.1007/S13562-019-00528-W

Shorangiz et al(2014) Shorangiz, Javanmardi, Arash, Azarpanah, Masoud, and Zadehbagheri. Proline Metabolite Transport an Efficient Approach in Corn Yield Improvement as Response to Drought Conditions. *American-Eurasian Journal of Agricultural and Environmental Sciences*. 2014;14:476-485.

Wang et al(2018)Wang, J.Y., Shi, D.H., Yu, B., Yang, D., Zhang, T., and Liu, Y. Effect of Drought Stress with PEG-6000 on Seed Germination and Physiological Properties in Abelmoschus esculentus. *Journal of Tropical and Subtropical Botany*. 2018.

Wang et al(2021) Wang, Y., Huang, L., Du F, Wang, J., Zhao, X., Li, Z., Wang, W., Xu, J., and Fu, B. Comparative transcriptome and metabolome profiling reveal molecular mechanisms underlying OsDRAP1-mediated salt tolerance in rice. *Scientific Reports*. 2021;11(1):5166. doi:10.1038/s41598-021-84638-3

Witt et al(2012) Witt, S., Galici, L., Lisec, J., Cairns, J., Tiessen, A., Araus, J.L., Palacios-Rojas, N., and Fernie, A.R. Metabolic and Phenotypic Responses of Greenhouse-Grown Maize Hybrids to Experimentally Controlled Drought Stress. *Molecular Plant*. 2012;5(2):401-417. doi:10.1093/mp/ssr102

Wójcik-Jaga et al(2020) Wójcik-Jaga, M., Rapacz, M., Dubas, E., Krzewska, M., and Ur, I. Candidate Genes for Freezing and Drought Tolerance Selected on the Basis of Proteome Analysis in Doubled Haploid Lines of Barley. *International Journal of Molecular Sciences*. 2020;21(6):2062. doi:10.3390/ijms21062062

Xiong et al(2019) Xiong, Q., Cao, C., Shen, T., Zhong, L., He, H.H., and Chen, X. Comprehensive metabolomic and proteomic analysis in biochemical metabolic pathways of rice spikes under drought and submergence stress. *Biochimica et Biophysica Acta (BBA) - Proteins & Proteomics*. 2019;1867(3):237-247. doi:10.1016/j.bbapap.2019.01.001

Yang et al(2019) Yang, J., Zhang, J., Li, C., Zhang, Z., and Li, M. Response of sugar metabolism in apple leaves subjected to short-term drought stress. *Plant Physiology and Biochemistry.* 2019;141:164-171. doi:10.1016/j.plaphy.2019.05.025

Zheng et al(2017) Zheng, Y., Liao, C., Zhao, S., Wang, C., and Guo, Y. The Glycosyltransferase QUA1 Regulates Chloroplast-Associated Calcium Signaling During Salt and Drought Stress in Arabidopsis. *Plant Cell Physiology*. 2017;58(2):329-341. doi:10.1093/pcp/pcw192

Zhong et al(2022) Zhong, Z.M., Zhang, J., Tang, B.G., Yu, F.F., Lu, Y.S., Hou, G., Chen, J.Y., and Du ZX. Transcriptome and metabolome analyses of the immune response to light stress in the hybrid grouper (Epinephelus lanceolatus male symbol x Epinephelus fuscoguttatus female symbol). *Animal*. 2022;16(2):100448. doi:10.1016/j.animal.2021.100448

Legends:

Table 1:

Separation gradient

Table 2:

The significantly ($P < 0.01$) enriched KEGG pathways

Table 3:

The list of nodes with both a high BC value (>0.02) and high degree value (>10)

Figure 1:

Global heatmap

Figure 2:

Statistics of DEPs from ten sample pairs: P2 versus P1, P3 versus P1, P3 versus P2, P4 versus P1, P4 versus P2, P4 versus P3, P5 versus P1, P5 versus P2, P5 versus P3, and P5 versus P4. Red: up-regulated expressed proteins, blue: down-regulated expressed proteins

Figure 3:

COG annotation

Figure 4:
Top 20 GO categories of all DEPs

Figure 5:
The most enriched GO terms in GO Slim

Figure 6:
Illustration of the PPI network A: The network of P2 versus P1, B: The network of P3 versus P1, C: The network of P4 versus P1, D: The network of P5 versus P1. Network nodes represent proteins. Edges represent protein-protein associations. The green nodes represent down-regulated DEPs, the red nodes represent up-regulated DEPs.

Figure 7:
Principal Component Analysis (PCA) of metabolite profiles A: PCA score plot in positive ion mode. B: PCA score plot in negative ion mode.

Figure 8:
Plots of PLS-DA score and permutation test. A: PLS-DA score plot in positive ion mode. B: PLS-DA score plot in negative ion mode. C: OPLS-DA permutation test plot in positive ion mode. D: OPLS-DA permutation test plot in negative ion mode.

Figure 9:
Plots of OPLS-DA score A: OPLS-DA score plot in positive ion mode. B: OPLS-DA score plot in negative ion mode.

Figure 1

Global heatmap

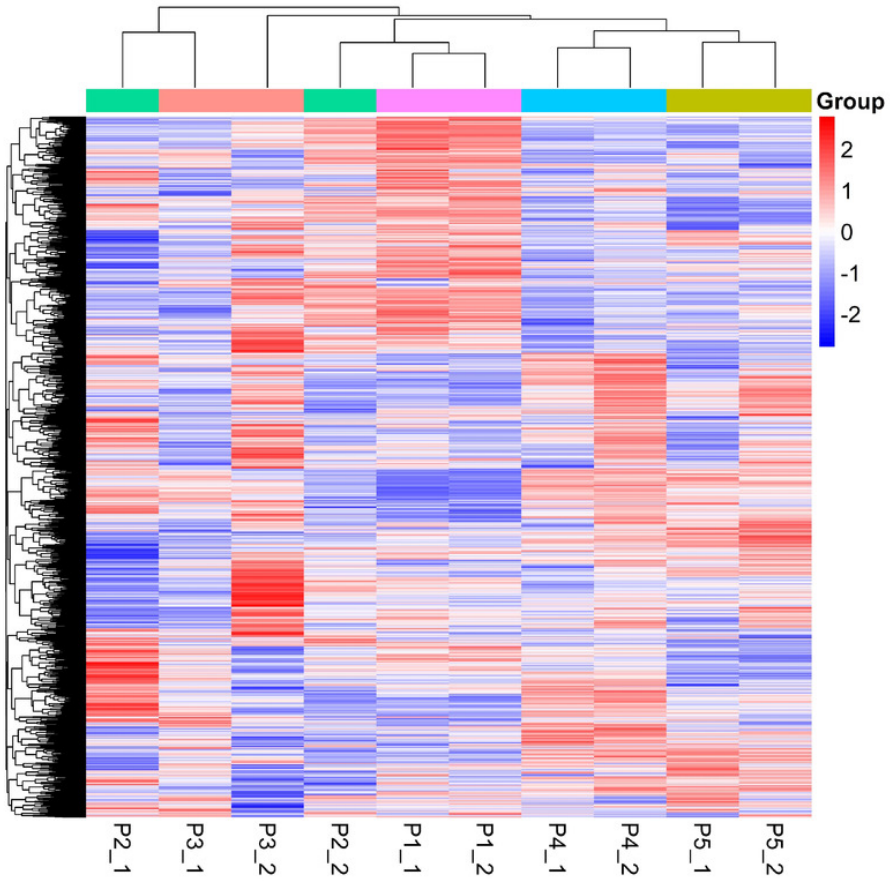
Group
2
1
0
-1
-2
P2_1
P3_1
P3_2
P2_2
P1_1
P1_2
P4_1
P4_2
P5_1
P5_2

Figure 2

Statistics of DEPs from ten sample-pairs, being namely P2 versus P1, P3 versus P1, P3 versus P2, P4 versus P1, P4 versus P2, P4 versus P3, P5 versus P1, P5 versus P2, P5 versus P3, and P5 versus P4. Red: upregulated expressed proteins, blue : down-reg

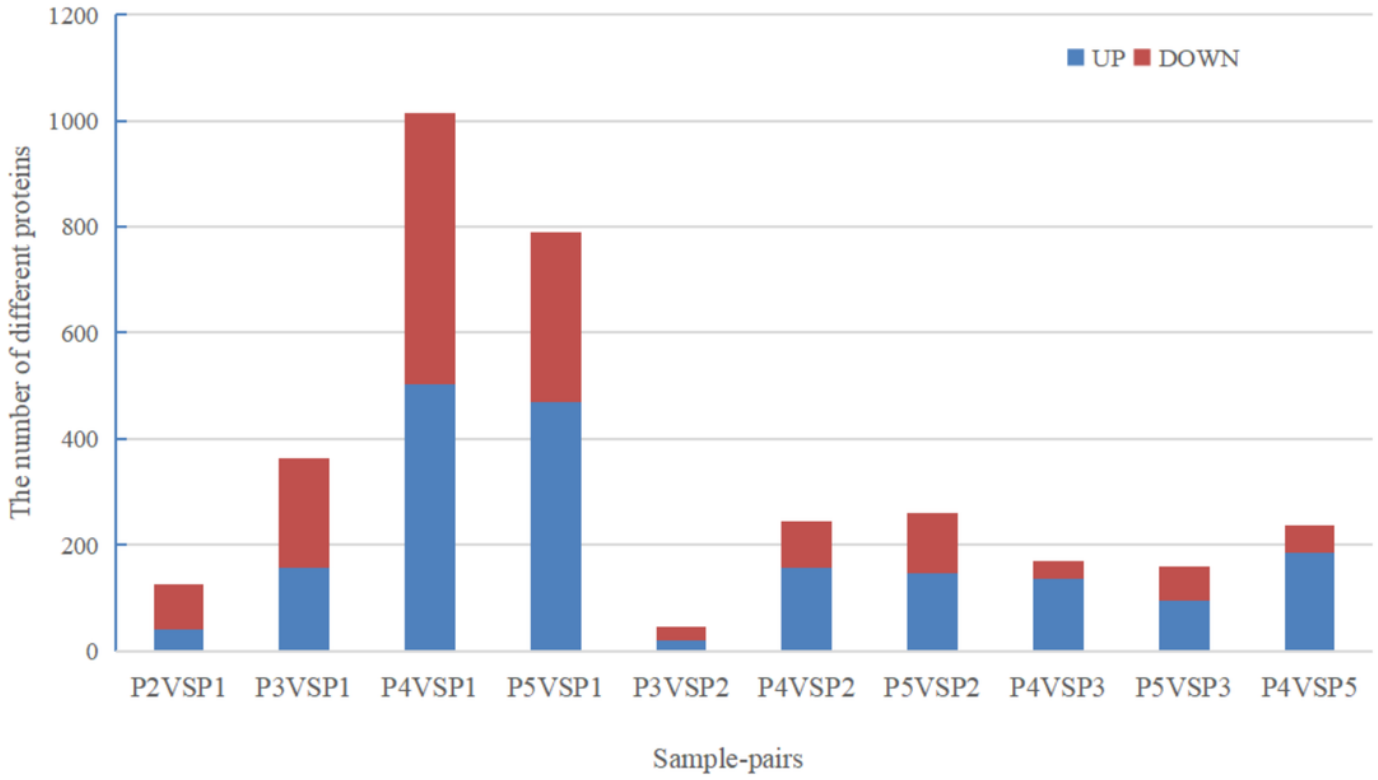

Figure 3

COG annotation

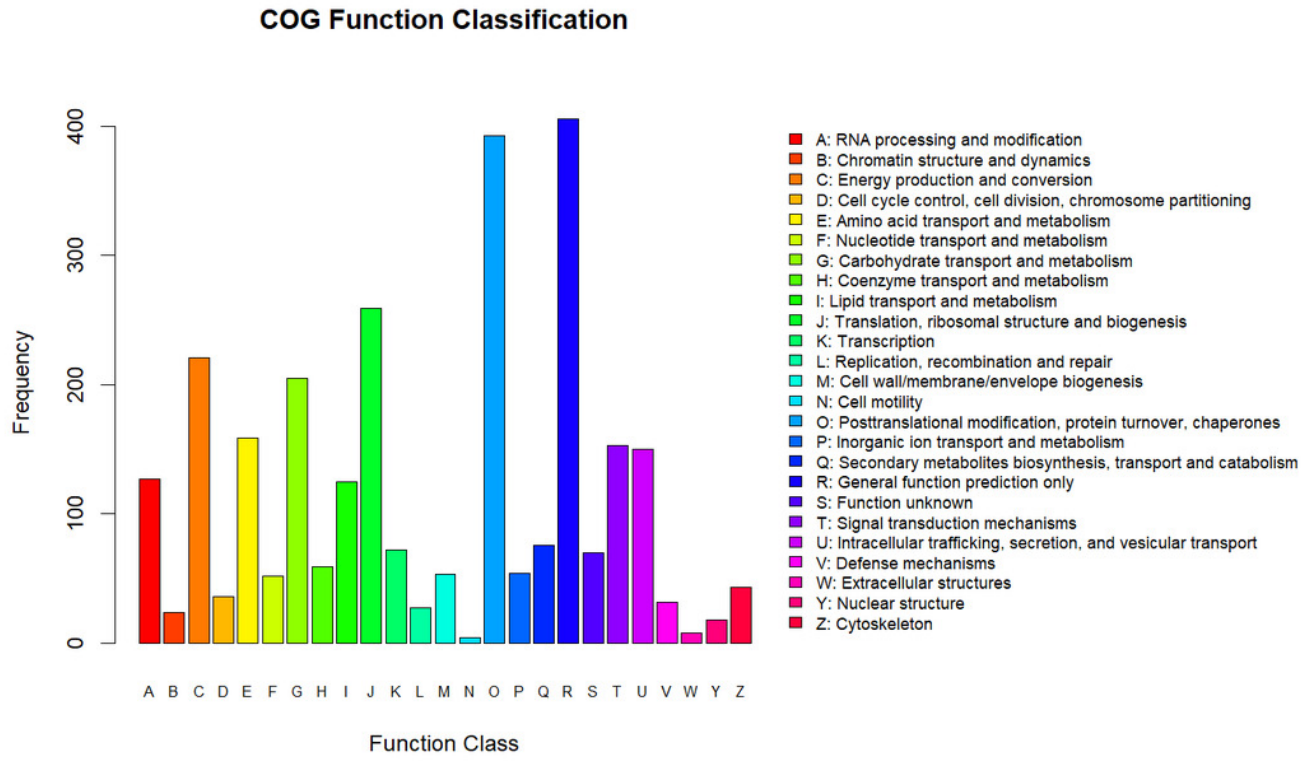

Figure 4

Top 20 GO categories of all DEPs

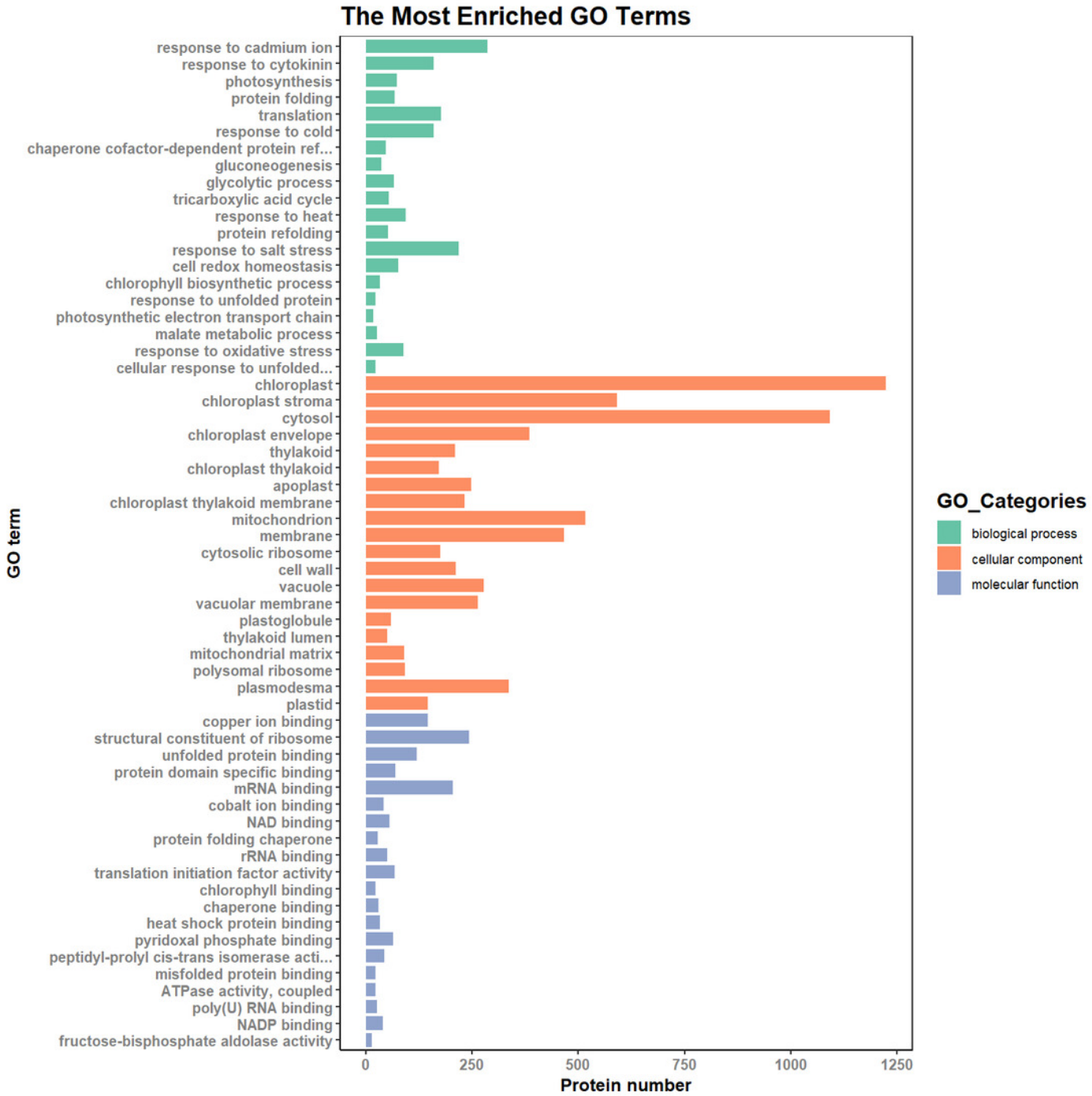

Figure 5

The most enriched GO terms in GO Slim

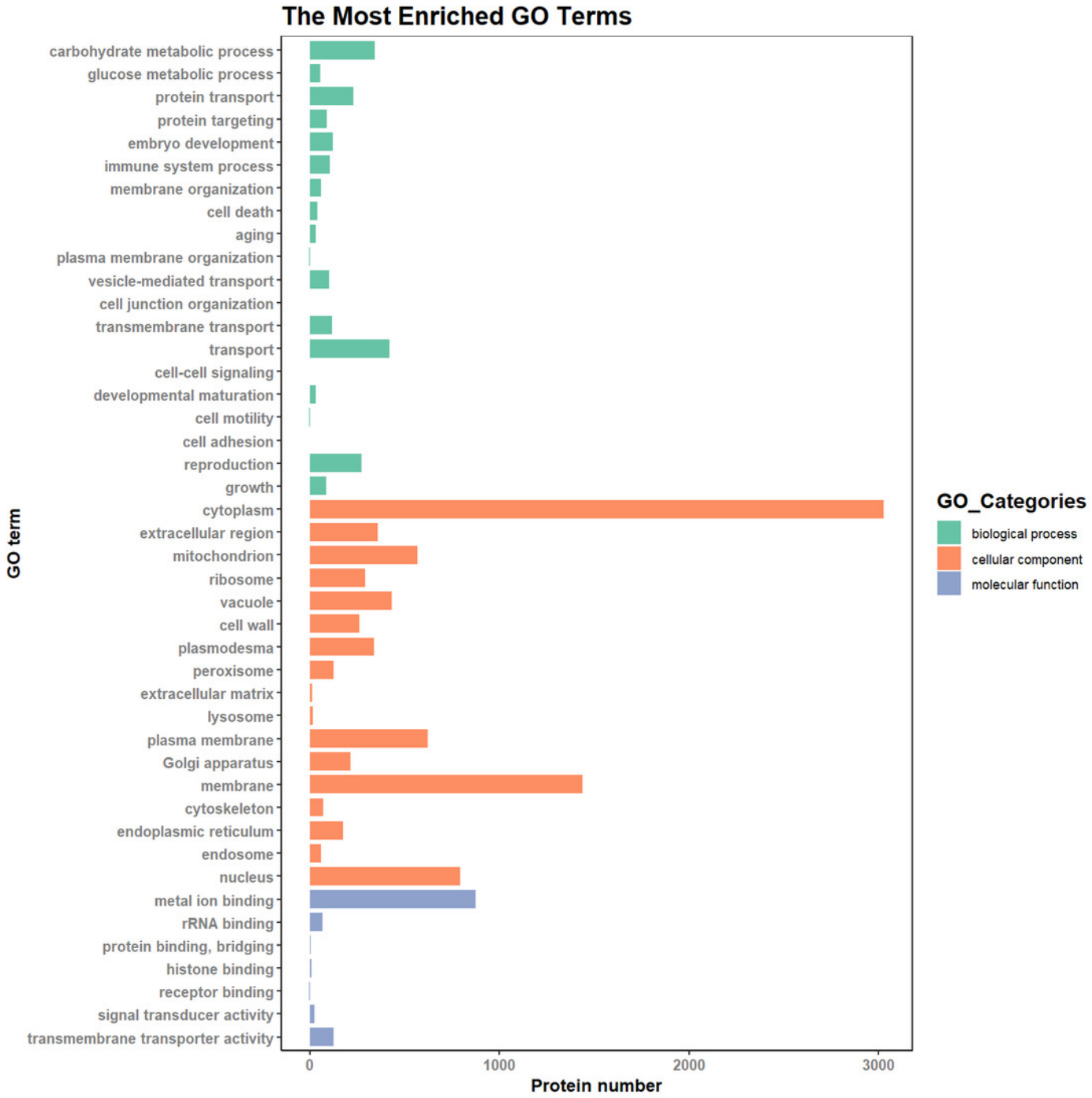

Figure 6

Illustration of the PPI network A: The network of P2 versus P1, B: The network of P3 versus P1, C: The network of P4 versus P1, D: The network of P5 versus P1. Network nodes represent proteins. Edges represent protein-protein associations. The green nodes

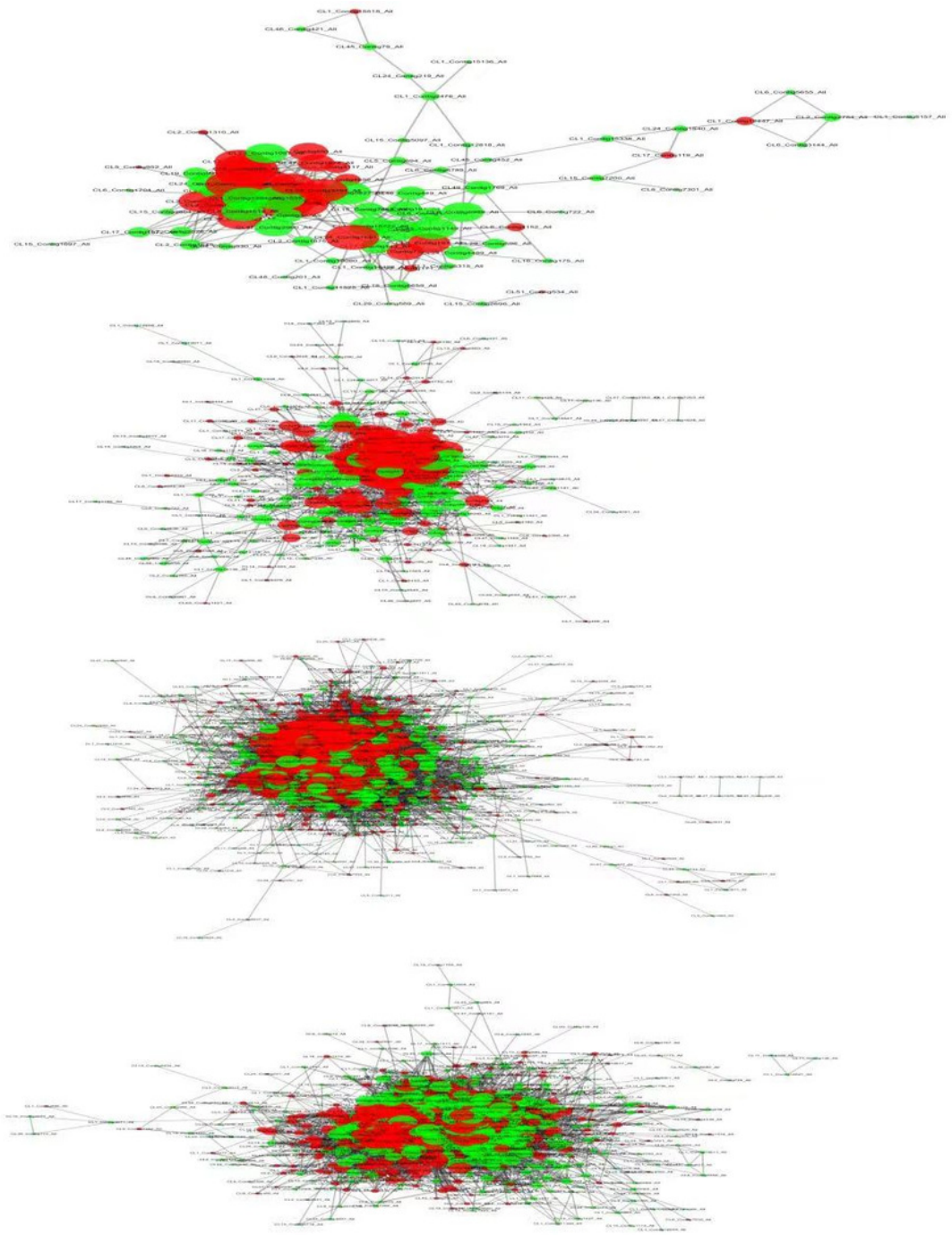

Figure 7

Principal Component Analysis (PCA) of metabolite profiles A: PCA score plot in positive ion mode. B: PCA score plot in negative ion mode.

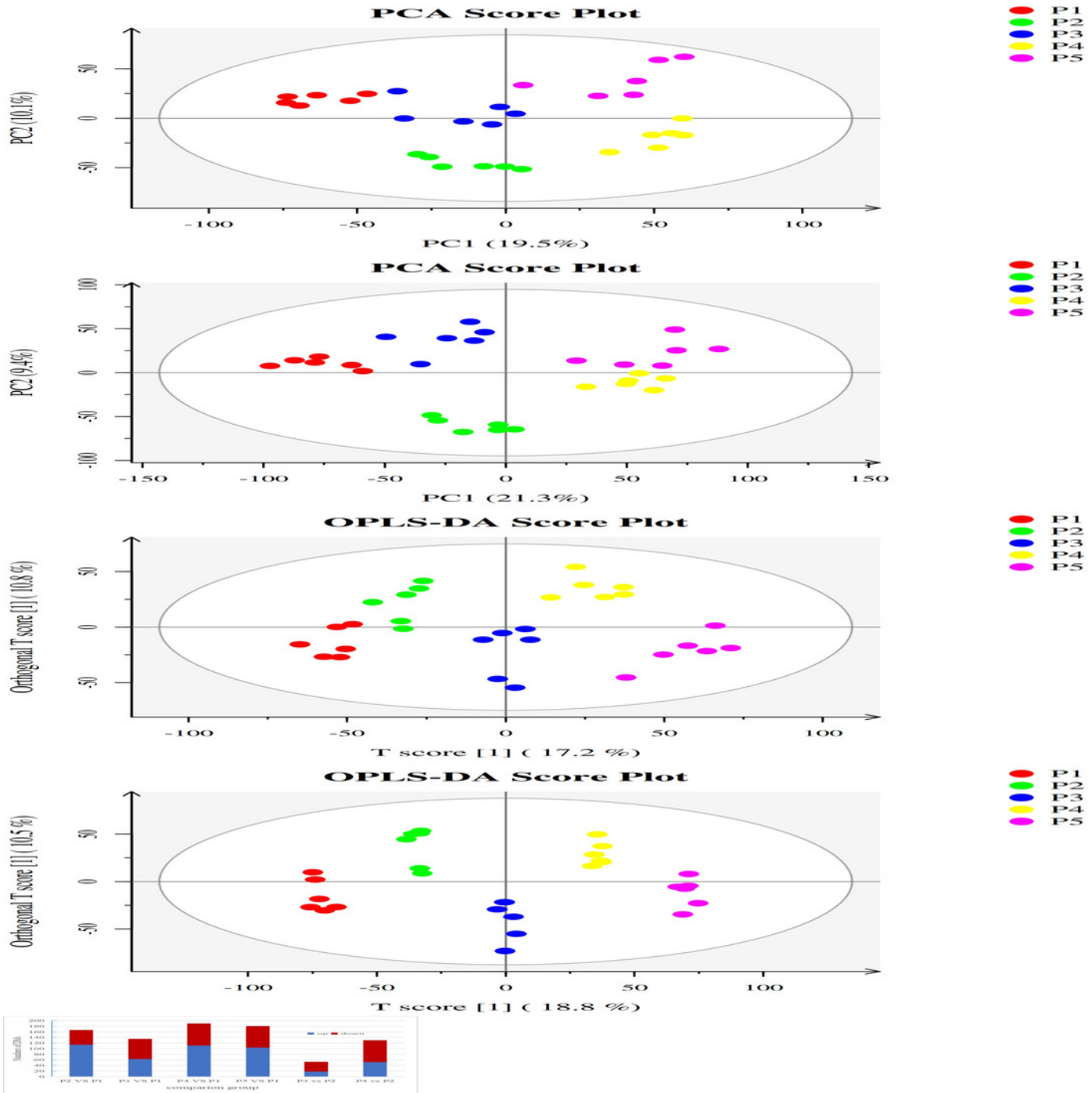

Figure 8

Plots of PLS-DA score and permutation test. A: PLS-DA score plot in positive ion mode. B: PLS-DA score plot in negative ion mode.C: OPLS-DA permutation test plot in positive ion mode. D:OPLS-DA permutation test plot in negative ion mode.

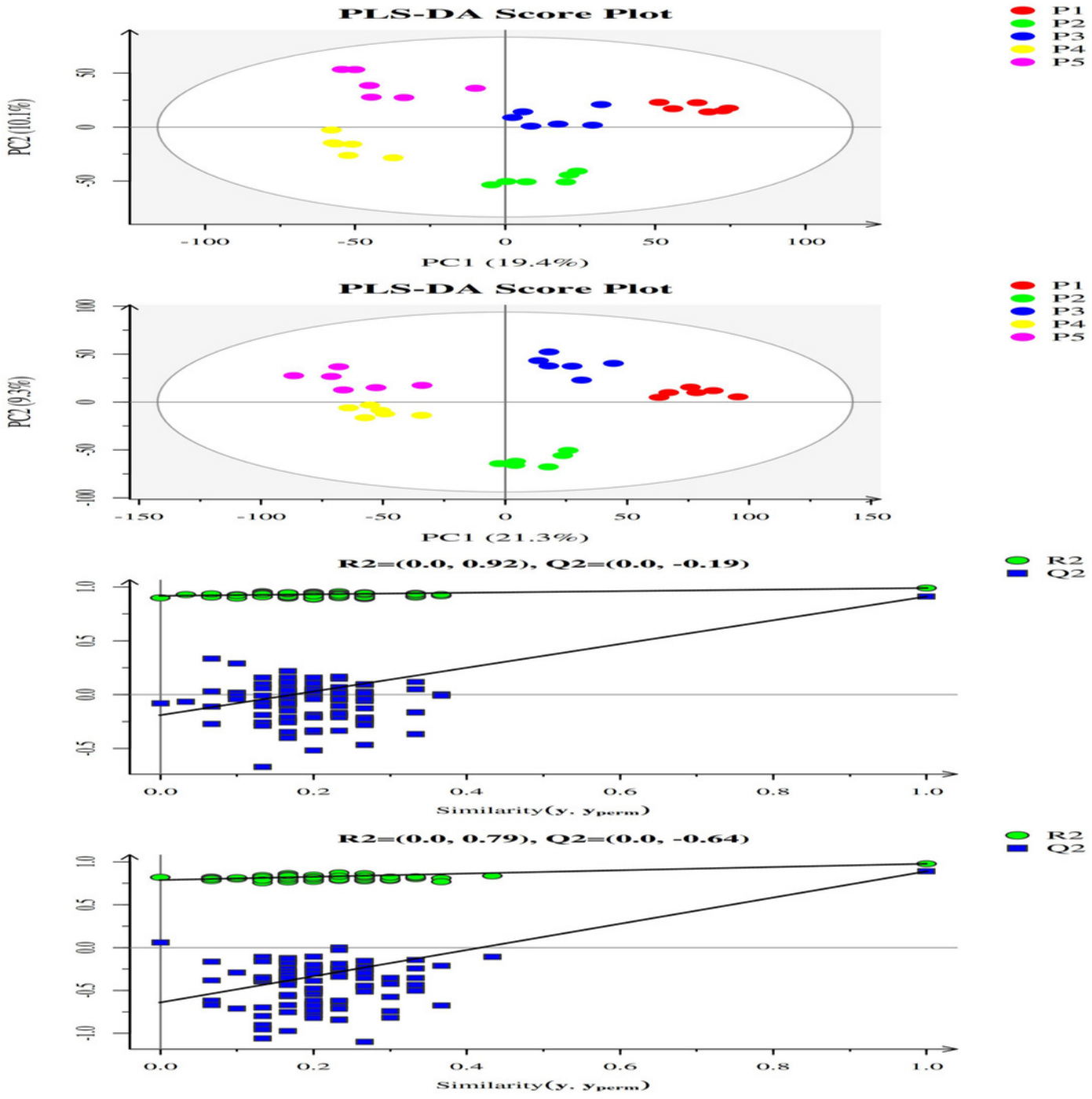

Figure 9

Plots of OPLS-DA scoreA: OPLS-DA score plot in positive ion mode. B:OPLS-DA score plot in negative ion mode.

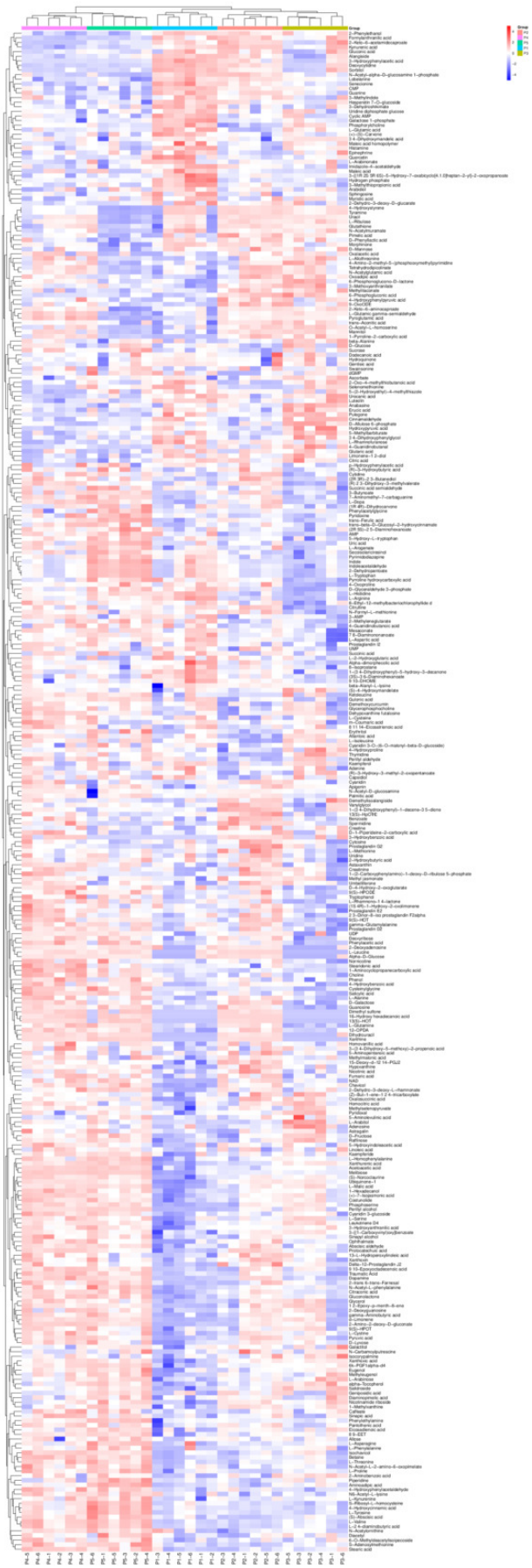

Table 1(on next page)

Separation gradient

1 Table 1 Separation gradient

Time (min)	Mobile phase A (0.1%FA/H_2O)	Mobile phase B (0.1%FA/ACN)
0	93%	7%
11	85%	15%
48	75%	25%
68	60%	40%
69	0%	100%
75	0%	100%

2

Table 2(on next page)

The significantly ($P < 0.01$) enriched KEGG pathways

1 Table 2 The significantly (P < 0.01) Enriched KEGG Pathways

Term ID	Term description	Termnum	P-value	Ratio	Enrichment	FDR
path:ath01100	Metabolic pathways	937	0.157346767	1.93E-26	25.7150997	2.41E-24
path:ath01110	Biosynthesis of secondary metabolites	557	0.163391024	2.15E-16	15.66656637	5.39E-15
path:ath01200	Carbon metabolism	238	0.234714004	2.88E-25	24.54112048	1.80E-23
path:ath03010	Ribosome	203	0.169449082	3.25E-07	6.487789383	2.90E-06
path:ath01230	Biosynthesis of amino acids	183	0.220481928	1.68E-16	15.77493564	5.25E-15
path:ath03040	Spliceosome	103	0.161189358	0.001667046	2.778052308	0.007185545
path:ath00010	Glycolysis / Gluconeogenesis	96	0.207343413	8.59E-08	7.065859234	9.76E-07
path:ath00620	Pyruvate metabolism	95	0.246753247	6.53E-12	11.18495109	1.17E-10
path:ath00710	Carbon fixation in photosynthetic organisms	85	0.307971014	1.15E-16	15.93857506	4.80E-15
path:ath00190	Oxidative phosphorylation	77	0.168859649	0.001769333	2.752190339	0.007372222
path:ath00630	Glyoxylate and dicarboxylate metabolism	73	0.253472222	5.13E-10	9.28984492	8.02E-09
path:ath00020	Citrate cycle (TCA cycle)	63	0.259259259	3.03E-09	8.518991062	4.20E-08
path:ath00260	Glycine, serine and threonine metabolism	60	0.256410256	1.12E-08	7.951195634	1.40E-07
path:ath00270	Cysteine and methionine metabolism	59	0.184952978	0.000659883	3.180532956	0.003299416
path:ath00195	Photosynthesis	58	0.364779874	2.14E-15	14.66871	4.47E-14
path:ath00230	Purine metabolism	56	0.178913738	0.001965531	2.706520092	0.007925528
path:ath00051	Fructose and mannose metabolism	54	0.215139442	1.93E-05	4.714206495	0.000127043
path:ath00970	Aminoacyl-tRNA biosynthesis	52	0.254901961	1.29E-07	6.891076785	1.34E-06
path:ath00480	Glutathione metabolism	52	0.228070175	4.85E-06	5.314302303	3.57E-05
path:ath01210	2-Oxocarboxylic acid metabolism	49	0.212121212	6.71E-05	4.173445821	0.000419212
path:ath03050	Proteasome	49	0.210300429	8.41E-05	4.074974554	0.00050086
path:ath01212	Fatty acid metabolism	49	0.17562724	0.005242324	2.280476165	0.019273249
path:ath00250	Alanine, aspartate and glutamate metabolism	47	0.262569832	1.99E-07	6.701294506	1.91E-06
path:ath00030	Pentose phosphate pathway	46	0.196581197	0.000666312	3.176322631	0.003203421
path:ath00053	Ascorbate and aldarate metabolism	39	0.276595745	5.08E-07	6.293861872	4.24E-06
path:ath00860	Porphyrin and chlorophyll metabolism	37	0.26618705	2.70E-06	5.568891264	2.11E-05
path:ath00280	Valine, leucine and isoleucine degradation	37	0.185	0.006096775	2.214899808	0.021774198
path:ath00061	Fatty acid biosynthesis	37	0.183168317	0.007176271	2.14410114	0.024917609
path:ath00592	alpha-Linolenic acid metabolism	36	0.204545455	0.001176924	2.929251557	0.005254125
path:ath00220	Arginine biosynthesis	28	0.24137931	0.000264729	3.577197832	0.001438747
path:ath00640	Propanoate metabolism	27	0.197080292	0.007622503	2.117902407	0.025751699
path:ath00670	One carbon pool by folate	20	0.298507463	9.32E-05	4.030622411	0.000529499
path:ath00290	Valine, leucine and isoleucine biosynthesis	18	0.25	0.002061633	2.685788684	0.008053253
path:ath00196	Photosynthesis	14	0.4375	8.45E-06	5.073151505	5.87E-05
path:ath00650	Butanoate metabolism	14	0.259259259	0.004375359	2.358986273	0.016573331
path:ath00300	Lysine biosynthesis	10	0.37037037	0.000836778	3.077389825	0.003873972
path:ath00261	Monobactam biosynthesis	9	0.409090909	0.000654796	3.183893939	0.003410396

2

Table 3(on next page)

The list of nodes with both a high BC value (>0.02) and high degree value (>10)

1 Table 3 The list nodes with both high BC(>0.02) and degree values(>10)

2

Pairs	Gene	BC value	D avlue
P2 versus P1	TPI [a]	0.1870093	19
	AT1G11860	0.17621229	17
	AT3G29320 [b]	0.12413995	13
	NRPB2 [d]	0.098109	17
	emb1473	0.09009896	25
	ACP4	0.08761633	18
	P5CS2 [f]	0.04926569	13
	NDPK2	0.04680682	13
	AT1G12230	0.0442739	15
	LOS2	0.04314511	15
	rps15	0.04216912	16
	AT2G43030	0.03732062	24
	PP2AA2	0.03569743	11
	GAPC1 [d]	0.03315947	13
P3 versus P1	CDC5[c]	0.14663404	40
	Hsp70b	0.10052988	38
	TPI [a]	0.05953945	41
	PSP	0.04886272	16
	AT3G29320 [b]	0.0481939	21
	NRPB2 [d]	0.04459201	41
	GS2 [e]	0.04413029	25
	CPN10	0.04098666	39
	LOX2	0.03694796	14
	mtLPD1	0.03669113	24
	AT1G09640	0.0346852	55
	CDPMEK	0.03296113	18
	GAPC1 [d]	0.03215865	26
	PUR5	0.0311079	38
P4 versus P1	CDC5 [c]	0.04350023	125
	TPI [a]	0.03028585	160
	AT3G29320 [b]	0.02679787	23
	P5CS2 [f]	0.02186006	118
	HSP70	0.02005322	158
P5 versus P1	CDC5 [c]	0.04774593	87
	AT5g06290	0.03391341	118
	TPI [a]	0.02928484	145
	HEME2	0.02682115	124

HSC70-1	0.0264096	84
AT3G54470	0.02636206	102
AT5G51970	0.02472014	67
GS2 [e]	0.02222725	70

Note a: Gene shared in all pairs.b: Gene shared in P2 versus P1, P3 versus P1, P4 versus P1. c: Gene shared in P3 versus P1, P4 versus P1, P5 versus P1. d:Gene shared in P2 versus P1, P3 versus P1. e:Gene shared in P3 versus P1 and P5 versus P1. f: Gene shared in P2 versus P1 and P4 versus P1.